Soil Parameters Dependency with Frequency – Its Influence in the Grounding Electrodes' Behaviour

Pedro António Aparício Vilela Dias
Instituto Superior Técnico
University of Lisbon
Lisbon, Portugal
pedro.aparicio.dias@tecnico.ulisboa.pt

June 2018

***Abstract*—After analysing and choosing the soil models to be considered, the response of simple grounding electrodes (vertical and horizontal) to lighting currents was simulated using the transmission line theory. These simulations were performed for both frequency dependant and independent models, for soils with low-frequency resistivities of 300 Ωm, 1000 Ωm and 4000 Ωm and for first and subsequent strokes. It was possible to verify that the dependence with frequency is responsible for the reduction of the magnitude of the harmonic impedance and for the increase of the capacitive effect. This causes the reduction of the grounding potential rise, the impulse impedance and the impulse coefficient, being this reduction more significant for soils with high resistivities and for subsequent strokes. It is also noticeable that the effective length, for first strokes, becomes larger when considering the frequency dependence, while for subsequent strokes there are not significant differences between the effective lengths of the frequency dependant and independent models. All these results show the importance of considering the frequency dependence of the soil parameters when studying the response of grounding electrodes to lightning currents.**

Keywords - Soil permittivity, soil resistivity, frequency dependence, grounding electrode, lightning current, transmission line theory.

I. INTRODUCTION

For many years the soil representation would assume its parameters to be frequency independent, both the resistivity and the permittivity, either for being common practice or simply because it was believed that the practical results would not be affected in a significant way. However, nowadays this is known to be incorrect, since these parameters are highly influenced by the variation of the frequency. As a result, this dependency will act on the way the grounding electrodes respond to a lightning stroke. Having this into consideration allows the creation of models that are able of accurately simulate the behaviour of grounding systems, which is essential to guarantee the security of people and infrastructures.

In a way of clarifying the dependency with the frequency of the soil parameters, each section will present one of the main elements of this study. So, in Section II, the soil parameters themselves will be introduced, as well as the different soil models capable of representing their variation with the frequency. Section III will include the study of the electrode, showing the equations needed to calculate the parameters of a horizontal and a vertical electrode, as well as the different models that can be adopted. The analytical representation of the lightning strokes will be shown in Section IV, along with the parameters that characterize the first and subsequent strokes measured at Morro do Cachimbo Station, in Brazil, and at San Salvatore Station, in Switzerland. Finally, in Section V, the results and simulations will be presented, being the conclusions taken during this study described in Section VI.

II. THE SOIL

To fully understand the behaviour of the soil, one has first to consider the parameters that characterize it. When the dependency with the frequency is not taken into consideration, both the soil resistivity (ρ) and the soil permittivity (ε) are assumed to be constant. The value assumed for the resistivity is, generally, the value measured at low-frequencies (ρ_0) and for the relative permittivity (ε_r) is usually between 2 and 80 [1]. Also, due to the high variability of these parameters, either because of the water content, the temperature or even the depth at which the measurements are taken, the soils of each region will be characterized by the median of the values measured during the year. However, since the frequency rise, result of the lightning stroke, will have a big impact on the soil parameters, the assumption that the parameters are constant often lead to inaccurate results [14].

To establish a correct soil model, several studies, based on experimental measurements, were performed in a way of deriving expressions capable of accurately representing the dependence of the soil parameters with the frequency. In this section, the equations of seven different soil models will be presented and divided in terms of their causality and behaviour along a specified frequency range.

A. Scott Model

One of the first studies addressing the dependency of the soil parameters with the frequency was presented by Scott in [1-2], where were obtained expressions that represent the soil's relative permittivity and conductivity (σ), which is the inverse of the resistivity, as a function of the frequency. These expressions are

$$\sigma(f) = 10^{K} \times 10^{-3} \tag{1a}$$

$$K = 0.028 + 1.098\log_{10}(\sigma_{100Hz}) - 0.068\log_{10}(f) + 0.036\log_{10}^{2}(\sigma_{100Hz}) - 0.046\log_{10}(f)\log_{10}(\sigma_{100Hz}) + 0.018\log_{10}^{2}(f) \tag{1b}$$

$$\varepsilon_r(f) = 10^{D} \tag{2a}$$

$$D = 5.491 + 0.946\log_{10}(\sigma_{100Hz}) - 1.097\log_{10}(f) + 0.069\log_{10}^{2}(\sigma_{100Hz}) - 0.114\log_{10}(f)\log_{10}(\sigma_{100Hz}) + 0.067\log_{10}^{2}(f) \tag{2b}$$

where f represents the frequency and σ_{100Hz} represents the soil conductivity, in [mS/m], measured at 100 Hz.

B. Smith-Longmire Model

By using Scott's measurements, Longmire and Longley presented, in [3], a new formulation for the parameters, which was later modified by Smith and Longmire in [4], where were included measurements by Wilkenfeld. The result were the expressions given by

$$\sigma(f) = \sigma_0 + 2\pi\varepsilon_0 \sum_{i=1}^{13} a_i F_i \frac{\left(\frac{f}{F_i}\right)^2}{1+\left(\frac{f}{F_i}\right)^2} \tag{3}$$

$$\varepsilon_r(f) = \varepsilon_\infty + \sum_{i=0}^{13} \frac{a_i}{1+\left(\frac{f}{F_i}\right)^2} \tag{4}$$

$$F_i = F(\sigma_0)\, 10^{i-1} \tag{5}$$

$$F(\sigma_0) = (125\sigma_0)^{0.8312} \tag{6}$$

where ε_0 is the vacuum permittivity ($\varepsilon_o \cong 8{,}854 \times 10^{-12}$ F/m), ε_∞ represents the limit of the relative permittivity at high-frequencies, assumed to be equal to 5, and σ_0 [S/m] represents the soil conductivity at low-frequencies which, in this case, is calculated by solving (3) for the specified value of σ_{100Hz} and for a frequency of 100 Hz. The coefficients a_i are listed in Table 1.

Table 1 – Coefficients a_i. (Values extracted from [4])

i	a_i	i	a_i
1	3.40×10^{6}	8	1.25×10^{1}
2	2.74×10^{5}	9	4.80×10^{0}
3	2.58×10^{4}	10	2.17×10^{0}
4	3.38×10^{3}	11	9.80×10^{-1}
5	5.26×10^{2}	12	3.92×10^{-1}
6	1.33×10^{2}	13	1.73×10^{-1}
7	2.72×10^{1}		

C. Messier Model

This model, also based on Scott's data, was initially demonstrated by Messier in [5] and later perfected in [6]. The expressions presented are

$$\sigma(f) = \sigma_0\left(1 + \sqrt{\frac{4\pi f\varepsilon_\infty}{\sigma_0}}\right) \tag{7}$$

$$\varepsilon_r = \frac{\varepsilon_\infty}{\varepsilon_0}\left(1 + \sqrt{\frac{\sigma_0}{\pi f\varepsilon_\infty}}\right) \tag{8}$$

Here, unlike the previous model, ε_∞ represents the permittivity at high frequencies and was defined as being equal to $8\varepsilon_0$. Also different from the Smith-Longmire model is the value of σ_0, which is assumed to be equal to σ_{100Hz} [S/m].

D. Visacro-Portela Model

This representation of the soil parameters was proposed by Visacro and Portela in [7] where, using their own measurements, the following expressions were obtained:

$$\sigma(f) = \sigma_0\left(\frac{f}{100}\right)^{0.072} \tag{9}$$

$$\varepsilon_r(f) = 2.34 \times 10^{6}\left(\frac{1}{\sigma_0}\right)^{-0.535} f^{-0.597} \tag{10}$$

where σ_0 is assumed to be equal to σ_{100Hz} [S/m].

E. Portela Model

One of the most used models was presented by Portela in [8], where, by using his own measurements, the author arrived at the expression given by

$$\sigma(f) \pm j\omega\varepsilon(f) = \sigma_0 + \Delta i\left[cot\left(\frac{\pi}{2}\alpha\right) \pm j\right]\left(\frac{\omega}{2\pi\times 10^{6}}\right)^{\alpha} \tag{11}$$

being ω the angular velocity ($\omega = 2\pi f$ rad/s) and σ_0 assumed to be equal to σ_{100Hz}. As for the statistical parameters, this work will use their median values, which are: $\Delta i = 11.71 \times 10^{-3}$ S/m and $\alpha = 0.706$, as indicated in [9].

F. Visacro-Alipio Model

In [10], Visacro and Alipio, based on their own data, created the following expressions:

$$\sigma(f) = \sigma_0\left\{1 + \left[1.2 \times 10^{-6}\left(\frac{1}{\sigma_0}\right)^{0.73}\right](f - 100)^{0.65}\right\} \tag{12}$$

$$\varepsilon_r(f) = 7.6 \times 10^{3}\, f^{-0.4} + 1.3 \;\text{ for }\; f \geq 10\text{kHz} \tag{13}$$

where σ_0 is assumed to be the same as σ_{100Hz}. It's also important to note that (12) is only valid for frequencies between 10 kHz and 4 MHz. For values lower than 10 kHz, Visacro and Alipio advise the use of the value obtained for 10 kHz.

G. Alipio-Visacro Model

More recently, Visacro and Alipio created a new model and presented it in [12]. There, they represented the frequency dependence of the soil parameters as

$$\sigma(f) = \left[\sigma_0 + \sigma_0\, h(\sigma_0) \left(\frac{f}{10^6}\right)^{\gamma}\right] \times 10^{-3} \qquad (14)$$

$$\varepsilon_r(f) = \frac{\varepsilon'_\infty}{\varepsilon_0} + \frac{\tan\left(\frac{\pi\gamma}{2}\right) 10^{-3}}{2\pi\varepsilon_0 (10^6)^{\gamma}} \sigma_0\, h(\sigma_0)\, f^{\gamma-1} \qquad (15)$$

where σ_0 [mS/m] is assumed to be equal to σ_{100Hz}. As for the parameters $h(\sigma_0)$, γ and $\varepsilon'_\infty/\varepsilon_0$, their values are indicated in Table 2. In this work were used the mean values.

Table 2 – Parameters of the Alipio-Visacro model. (Extracted from [12])

	$h(\sigma_0)$	γ	$\varepsilon'_\infty/\varepsilon_0$
Mean results	$h_1 = 1.26 \times \sigma_0^{-0.73}$	0.54	12
Relatively conservative results	$h_2 = 0.95 \times \sigma_0^{-0.73}$	0.58	8
Conservative results	$h_3 = 0.70 \times \sigma_0^{-0.73}$	0.62	4

➢ *Comparison of the Models*

In a way of comparing the different soil models, one must address both their causality and their overall results in the frequency domain. The causality of the first six models was addressed in [13] where, by applying the Kramers-Kronig relationships, it was possible to determine the following models as causal: Smith-Longmire, Messier and Portela. As for the Alipio-Visacro model, its causality was analysed in [11], from where was concluded that its curves are in agreement with the Kramers-Kronig relationships, thus proving its causality.

After simulating the models' expressions in MATLAB, the curves of both resistivity and relative permittivity were obtained and presented in Figs. 1-3.

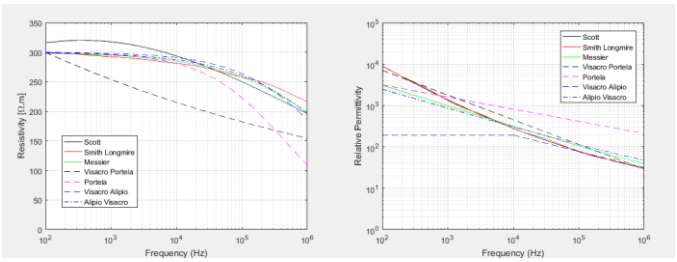

Fig. 1 – Comparison of the resistivity (left) and the relative permittivity (right) of the different soil models ($\rho_{100Hz} = 300\ \Omega m$).

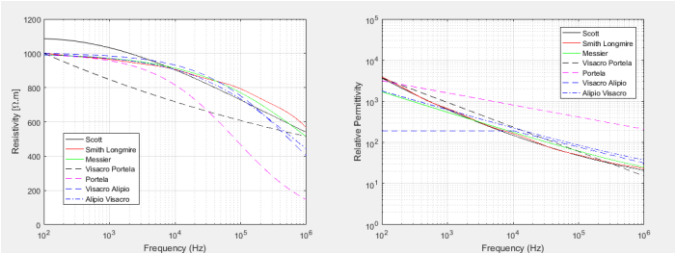

Fig. 2 – Comparison of the resistivity (left) and the relative permittivity (right) of the different soil models ($\rho_{100Hz} = 1000\ \Omega m$).

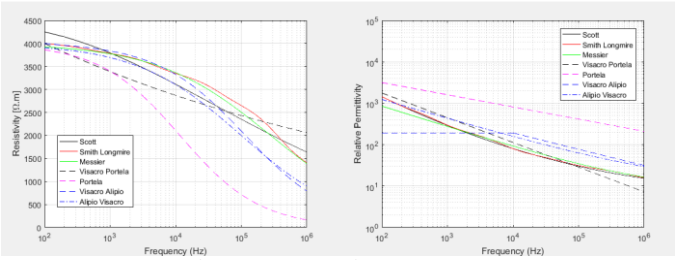

Fig. 3 – Comparison of the resistivity (left) and the relative permittivity (right) of the different soil models ($\rho_{100Hz} = 4000\ \Omega m$).

For all models, as the frequency rises, both the values of resistivity and relative permittivity decrease. In the case of the resistivity, this happens because, as the frequency rises, the values for the current density, in the soil, increase, which causes the lowering of the resistivity. As for the permittivity, it presents, for low-frequencies, very high values, being the molecules of the soil highly polarized. So, since the frequency rise hinders the polarization phenomenon, the value of the permittivity will suffer a significant reduction.

By analysing the curves, it can be seen that, while the Visacro-Portela and Portela models have a different behaviour than the rest, probably due to the different set of data they´re based on, the other soil models predict similar results. It is also noticeable that the models start to differ more from one another at high-frequencies and for higher values of ρ_{100Hz}.

Having all the above results into consideration, it was possible to determine which soil models will be used in the simulations. Those models are: Smith-Longmire, Messier, Portela, Visacro-Alipio and Alipio-Visacro. Note that, even though the Visacro-Alipio model didn´t pass the causality tests and the Portela model presents a different behaviour than the rest, since they're highly popular, both will be considered.

III. The Electrode

The creation of simulations capable of accurately representing a grounding system depends heavily on a rigorous analytical representation of the electrode's parameters. Only by doing this is it possible to determine the system's impedance and, consequently, the potential developed during a lightning strike. However, choosing the right approach is not an easy task, since it has, not only to be accurate, but also of practical implementation. Of all the existing approaches, the ones that stand out the most in the literature are:

- The Circuit Approach [20-25], where the electrode is represented, or by a resistance [Fig. 4(a)], in a low-frequency case, or by a lumped R-L-C circuit [Fig. 4(b)], in a high-frequency case, or even by a segmented R-L-C circuit [Fig. 4(c)]. Then, by solving the nodal equations, simple expressions, capable of representing the grounding system, are obtained.
- The Electromagnetic Field Approach [27-32], which is the most accurate method and often used to validate other approaches, since it requires fewer approximations than other methods. Even so, because it requires the system to be linear, phenomena like soil ionization (which will not be considered in this study) cannot be represented.
- The Hybrid Approach [33-37], which is a combination of both the circuit and the electromagnetic approaches. It achieves very accurate results while at the same time represents the system in a simpler way than the electromagnetic field approach.
- The Transmission-Line Approach [38-41], where the electrode is represented as a lossy transmission-line, divided into N sections [Fig. 4(c)], each section being characterized by a resistance, an inductance and a capacitance.

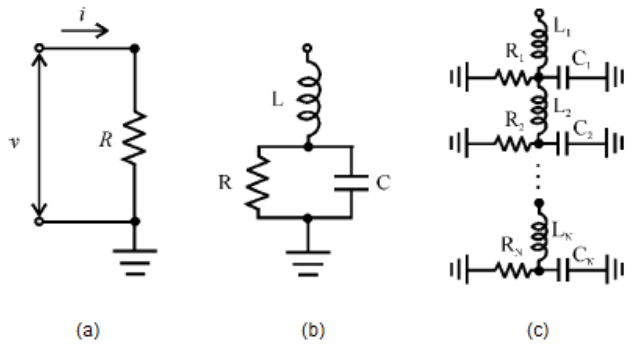

Fig. 4 – Grounding electrode models. (a) Low-frequency resistance. (b) High-frequency lumped R-L-C circuit. (c) High-frequency segmented R-L-C circuit. (Extracted from [26])

From all the above approaches, it was selected the transmission-line method, since both the electromagnetic field approach and the hybrid approach are very complex and of difficult implementation, and the circuit approach is not as accurate as the transmission-line approach [26].

Having chosen the method, it is time to calculate the line parameters R, L and C. From consulting the works of Dwight [42] and Sunde [18], it was possible to determine the expressions that represent the parameters of a vertical and horizontal electrode.

For a vertical electrode, of length l and radius a, the equations of its parameters are:

$$R = \frac{\rho}{2\pi l}\left[\ln\left(\frac{4l}{a}\right) - 1\right] \quad (16)$$

$$C = \frac{2\pi l\varepsilon}{\ln\left(\frac{4l}{a}\right)-1} \quad (17)$$

$$L = \frac{\mu l}{2\pi}\left[\ln\left(\frac{2l}{a}\right) - 1\right] \quad (18)$$

where μ is the magnetic permeability of the soil, which is assumed to be equal to the vacuum permeability (μ_0).

For a horizontal electrode, of length l, radius a and buried at a depth of d, the equations are:

$$R = \frac{\rho}{\pi l}\left[\ln\left(\frac{2l}{\sqrt{2ad}}\right) - 1\right] \quad (19)$$

$$C = \frac{\pi l\varepsilon}{\ln\left(\frac{2l}{\sqrt{2ad}}\right)-1} \quad (20)$$

$$L = \frac{\mu l}{2\pi}\left[\ln\left(\frac{2l}{\sqrt{2ad}}\right) - 1\right] \quad (21)$$

However, it is often used (18) for both the horizontal and vertical electrodes' inductances, as indicated in [18].

Finally, the per-unit-length parameters G', L' and C', are given by

$$G' = 1/Rl \quad (22)$$

$$C' = C/l \quad (23)$$

$$L' = L/l \quad (24)$$

These parameters will be necessary to calculate the harmonic grounding impedance, which will be calculated at the input of the transmission-line and considering an open circuit. The analytical expression of the harmonic impedance is obtained through the transmission-line equations

$$\bar{U}(z) = \bar{U}_i e^{-\bar{\gamma}z} + \bar{U}_r e^{\bar{\gamma}z} \quad (25)$$

$$\bar{I}(z) = \frac{\bar{U}_i}{\bar{Z}_w} e^{-\bar{\gamma}z} - \frac{\bar{U}_r}{\bar{Z}_w} e^{\bar{\gamma}z} \quad (26)$$

being $\bar{U}(z)$ and $\bar{I}(z)$ the complex amplitudes of the voltage and current, respectively, at a position z in the line, $\bar{U}_i$ the complex amplitude of the incident wave's voltage and $\bar{U}_r$ the complex amplitude of the reflected wave's voltage. $\bar{Z}_w$ and $\bar{\gamma}$ are the frequency dependent parameters, the characteristic impedance and the propagation constant, respectively, which are defined by the equations

$$\bar{Z}_w = \sqrt{\frac{j\omega L'}{G'+j\omega C'}} \quad (27)$$

$$\bar{\gamma} = \sqrt{j\omega L'(G' + j\omega C')} \quad (28)$$

Then, by solving (25) and (26) at the input of the line ($z = 0$), and then again assuming an open circuit at the end of the line [$\bar{I}(z = l) = 0$], it can be obtained the equation given by

$$\overline{U}(z = 0) = \overline{Z}_w \coth(\overline{\gamma} l)\, \bar{I}(z = 0) \qquad (29)$$

where $\overline{U}(z = 0)$ is the potential developed at the input and $\bar{I}(z = 0)$ is the incident current, both as a function of frequency. And so, the harmonic grounding impedance is given by

$$\overline{Z}(\omega) = \overline{Z}_w \coth(\overline{\gamma} l) \qquad (30)$$

being l the total length of the electrode.

IV. The Lightning Current

Due to the probabilistic nature of lightning strokes, a correct analytical representation can be a challenge. As a way of determining which types of strokes are the most common, CIGRE (International Council on Large Electric Systems) gathered measurements from all around the world, presenting, in [46], the values for the lightning parameters.

CIGRE also adopted the waveform proposed by Anderson and Eriksson in [47, p. 85], which is a negative downward stroke. Another characteristic of the lightning strokes, that became evident by analysing the data, was that most lightning flashes contain multiple strokes, more specifically, one double-peaked first stroke, followed by one or more single-peaked subsequent stroke.

In this work, the values for the parameters of first and subsequent stroke taken into consideration are the ones measured at San Salvatore, in Switzerland, and at Morro do Cachimbo, in Brazil, which are indicated in Tables 3-4.

Table 3 – Median parameters of the first and subsequent strokes, measured at San Salvatore Station. (Values extracted from [47])

Type	I_{p1} [kA]	I_{p2} [kA]	T_{10} [μs]	T_{30} [μs]	T_{50} [μs]	S_{10} [kA/μs]	S_{30} [kA/μs]	$(di/dt)_{max}$ [kA/μs]
First stroke	27.7	31.1	4.5	2.3	75.0	5.0	7.2	24.3
Sub. stroke	11.8	-	0.6	0.4	32.0	15.4	20.1	39.9

Table 4 – Median parameters of the first and subsequent strokes, measured at Morro do Cachimbo Station. (Values extracted from [49])

Type	I_{p1} [kA]	I_{p2} [kA]	T_{10} [μs]	T_{30} [μs]	T_{50} [μs]	S_{10} [kA/μs]	S_{30} [kA/μs]	$(di/dt)_{max}$ [kA/μs]
First stroke	40.4	45.3	5.6	2.9	53.5	5.8	8.4	19.4
Sub. stroke	16.3	-	0.7	0.4	16.4	18.7	24.7	29.9

The names of the parameters shown are the following:

I_{p1} – first peak maximum amplitude;

I_{p2} – second peak maximum amplitude;

T_{10} – front time between 10% and 90% of the first peak maximum amplitude;

T_{30} – front time between 30% and 90% of the first peak maximum amplitude;

T_{50} – time it takes for the current amplitude to decay 50% of the second peak maximum amplitude;

S_{10} – average current steepness between 10% and 90% of the first peak maximum amplitude;

S_{30} – average current steepness between 30% and 90% of the first peak maximum amplitude.

$(di/dt)_{max}$ – maximum rising rate of the current.

➢ *Analytical Representation of the lightning strokes*

In an attempt of mathematically representing curves with the characteristics of the lightning strokes, Heidler proposed, in [50], a new expression called Heidler function where, by summing and adjusting multiple functions, it is possible to obtain the desired current waveforms. This sum of Heidler functions is given by

$$i(t) = \sum_{k=1}^{m} \left(\left(\frac{I_{0k}}{\eta_k}\right) e^{\left(\frac{-t}{\tau_{2k}}\right)} \left(\frac{\left(\frac{t}{\tau_{1k}}\right)^{n_k}}{1+\left(\frac{t}{\tau_{1k}}\right)^{n_k}} \right) \right) \qquad (31a)$$

$$\eta_k = e^{-\left(\frac{\tau_{1k}}{\tau_{2k}}\right)\left(\frac{n_k \tau_{2k}}{\tau_{1k}}\right)^{\frac{1}{n_k}}} \qquad (31b)$$

So, in a way of obtaining curves with the characteristics indicated in Tables 3-4, one must use the Heidler function's parameters presented in Tables 5-6, which were extracted from [51].

Table 5 – Parameters of the seven Heidler functions needed to represent the median values of the first strokes, measured at San Salvatore Station and Morro do Cachimbo Station. (Values extracted from [51])

	San Salvatore				**Morro do Cachimbo**			
k	I_{0k} [kA]	n_k	τ_{1k} [μs]	τ_{2k} [μs]	I_{0k} [kA]	n_k	τ_{1k} [μs]	τ_{2k} [μs]
1	3.0	2.0	3.0	76.0	6.0	2.0	3.0	76.0
2	4.5	3.0	3.5	25.0	5.0	3.0	3.5	10.0
3	3.0	5.0	5.2	20.0	5.0	5.0	4.8	30.0
4	3.8	7.0	6.0	60.0	8.0	9.0	6.0	26.0
5	13.6	44.0	6.6	60.0	16.5	30.0	7.0	23.2
6	11.0	2.0	100.0	600.0	17.0	2.0	70.0	200.0
7	5.7	15.0	11.7	48.5	12.0	14.0	12.0	26.0

Table 6 – Parameters of the two Heidler functions needed to represent the median values of the subsequent strokes, measured at San Salvatore Station and Morro do Cachimbo Station. (Values extracted from [51])

	San Salvatore				Morro do Cachimbo			
k	I_{0k} [kA]	n_k	τ_{1k} [μs]	τ_{2k} [μs]	I_{0k} [kA]	n_k	τ_{1k} [μs]	τ_{2k} [μs]
1	10.7	2.0	0.25	2.5	15.4	3.4	0.6	4.0
2	6.5	2.0	2.1	230.0	7.2	2.0	4.0	120.0

Finally, by plotting the equations in MATLAB, are obtained the curves which will be used to simulate the response of the grounding electrodes. These curves are presented in Figs. 5-6.

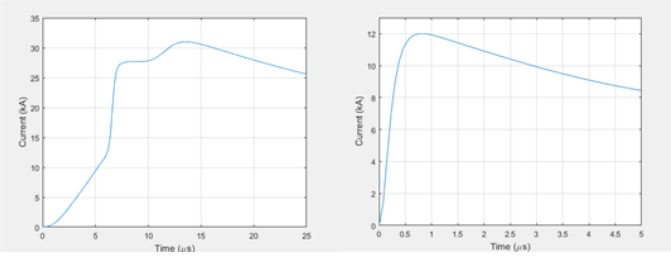

Fig. 5 – Waveforms of the first stroke (left) and the subsequent stroke (right) simulated for the values measured at San Salvatore Station.

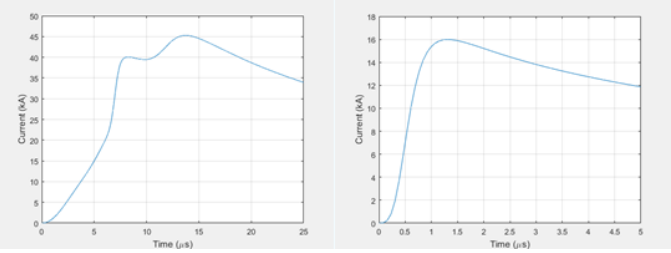

Fig. 6 – Waveforms of the first stroke (left) and the subsequent stroke (right) simulated for the values measured at San Salvatore Station.

V. THE ELECTRODE'S RESPONSE

This section will present the several parameters that characterize the electrode's response to a lightning stroke, which are: the harmonic grounding impedance, the grounding potential rise (GPR), the impulse impedance, the impulse coefficient and the effective length. These parameters are obtained through MATLAB simulations and shown in plots that include, not only the soil models adopted in Section II, but also the curves for the frequency independent model, characterized by constant soil parameters, being the resistivity equal to the value of ρ_0 and the relative permittivity assumed to be equal to 10, which is the value often used in these type of studies [14].

➢ *Response Parameters*

The harmonic grounding impedance, $\overline{Z}(\omega)$, as referred in Section III, was calculated at the electrode's input, which is the point where the lightning strikes, and is given by (30).

The GPR represents, in the time domain, the voltage $u(t)$ developed at the input, in response to the injected lightning current $i(t)$. This parameter is calculated by performing an Inverse Fast Fourier Transform (IFFT) in (29), where the term $\overline{I}(z=0)$ is obtained by using the Fast Fourier Transform (FFT) algorithm in the current $i(t)$.

Having the time domain curves for both the GPR and the lightning current, it can be obtained, for a certain electrode length, the respective impulse impedance, Z_p, which is given by

$$Z_p = V_p / I_p \tag{32}$$

being V_p the maximum value for the voltage and I_p the maximum value for the lightning current.

As for the impulse coefficient, I_c, it corresponds to the ratio between the impulse impedance and the low-frequency resistance, R_{LF}, as indicated by

$$I_C = Z_p / R_{LF} \tag{33}$$

This low-frequency resistance is simulated by using the expressions for the resistance indicated in Section III, for a constant value of soil resistivity, which will correspond to the value of ρ_0.

Finally, it's possible to determine the effective length of the electrode, L_{EF}, either by checking the length from which the reduction of the impulse impedance stops being noticeable, or by seeing the length at which the impulse coefficient starts to increase.

➢ *Simulation and Results*

The simulations presented in this paper are for a horizontal electrode with the characteristics indicated in Table 7, and for three types of soils: 300 Ωm (low-resistivity soil), 1000 Ωm and 4000 Ωm (high-resistivity soil). The results will be presented for the first and subsequent strokes measured at Morro do Cachimbo.

Table 7 – Characteristics of the simulated electrode.

Electrode			
Type	l [m]	a [m]	d [m]
Horizontal	30	0,007	0,5

1) Harmonic Grounding Impedance

The module and phase of the harmonic grounding impedance are shown in Figs. 7-9, for the three soil types and for a frequency range of 100 Hz to 4 MHz.

According to the figures, when the frequency dependence is considered, the module of the impedance, after a certain frequency, suffers a significant reduction, when compared to the model with constant soil parameters. This dependency is also responsible for the intensification of the capacitive effect,

characterized by the negative values observed in the harmonic impedance's phase.

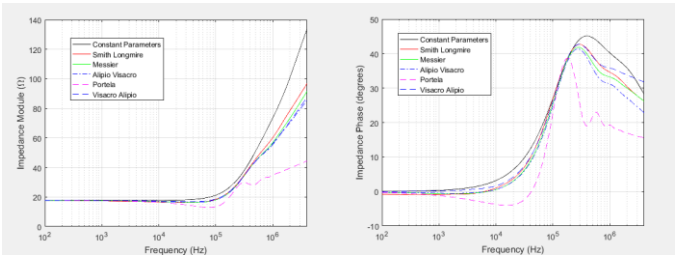

Fig. 7 – Module (left) and phase (right) of the harmonic impedance for the electrode described in Table 7, buried in a soil with $\rho_0 = 300$ Ωm

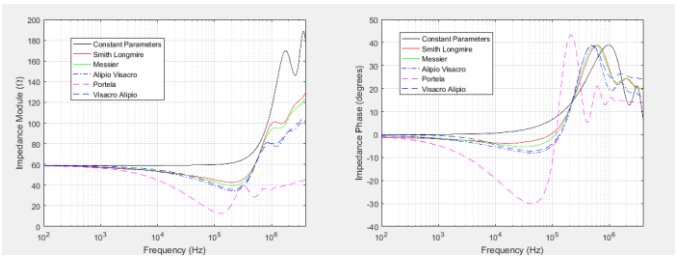

Fig. 8 – Module (left) and phase (right) of the harmonic impedance for the electrode described in Table 7, buried in a soil with $\rho_0 = 1000$ Ωm

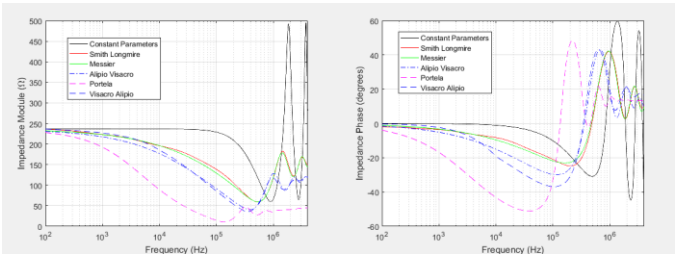

Fig. 9 – Module (left) and phase (right) of the harmonic impedance for the electrode described in Table 7, buried in a soil with $\rho_0 = 4000$ Ωm

Also, both the capacitive effect and the reduction of the impedance's amplitude are amplified for high-resistivity soils, which also causes the lowering of the frequency from which these effects are noticeable. This happens because, as it can be seen in Figs. 1-3, the reduction of the resistivity is more abrupt for higher values of ρ_0 while, at the same time, the relative permittivity presents values much higher than the ones usually assumed.

2) Grounding Potential Rise

The GPR is represented in Figs. 10-12, for the three types of soil and for the first and subsequent strokes measured at Morro do Cachimbo.

The reduction of the GPR values, when considering the frequency dependence, occurs because of the reduction of the resistivity values, which is responsible for the higher reduction of the voltage. It is also evident that this reduction is more pronounced for high-resistivity soils since, as it was already said, the effects of the frequency dependence in these soils are more significant and start for lower frequency values. This is also the cause for higher reduction along the wave tail, for high-resistivity soils, when compared to the wave tails for low-resistivity soils, where the reduction is less significant.

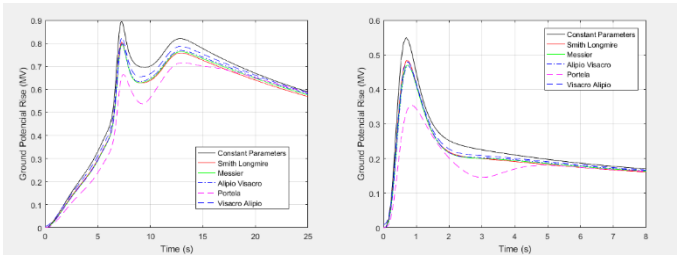

Fig. 10 – GPR of the electrode described in Table 7, subjected to a first stroke (left) and a subsequent stroke (right), in a soil with $\rho_0 = 300$ Ωm.

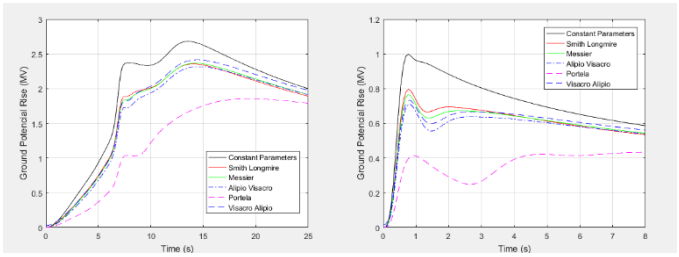

Fig. 11 – GPR of the electrode described in Table 7, subjected to a first stroke (left) and a subsequent stroke (right), in a soil with $\rho_0 = 1000$ Ωm.

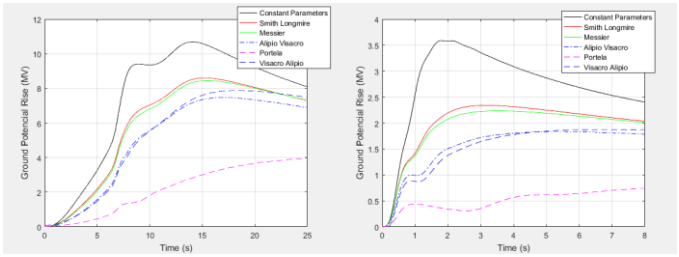

Fig. 12 – GPR of the electrode described in Table 7, subjected to a first stroke (left) and a subsequent stroke (right), in a soil with $\rho_0 = 4000$ Ωm.

In addition, the reduction of the GPR is greater for subsequent strokes since, due to the shorter rise-times, these strokes present higher frequency components than the first strokes, which causes the intensification of the capacitive effect and the reduction of the resistivity.

3) Impulse Impedance

Having been obtained the values of the impulse impedance for different electrode lengths, it was possible to simulate the curves from Figs. 13-15, which represent this parameter's variation for the three types of soil considered and for a first and subsequent strokes.

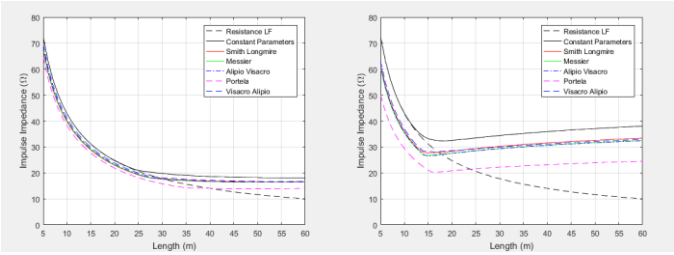

Fig. 13 – Variation of the impulse impedance with the length of the electrode described in Table 7, subjected to a first stroke (left) and subsequent stroke (right), for a soil with $\rho_0 = 300$ Ωm.

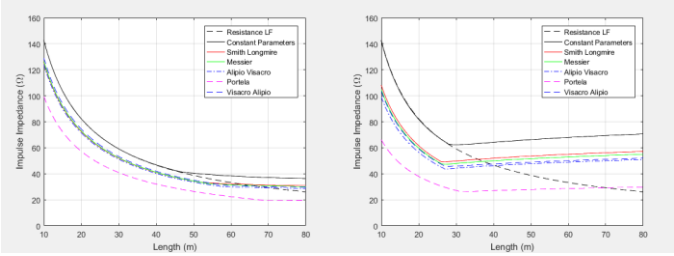

Fig. 14 – Variation of the impulse impedance with the length of the electrode described in Table 7, subjected to a first stroke (left) and subsequent stroke (right), for a soil with $\rho_0 = 1000$ Ωm.

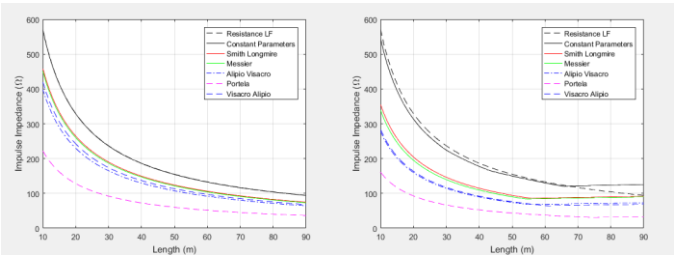

Fig. 15 – Variation of the impulse impedance with the length of the electrode described in Table 7, subjected to a first stroke (left) and subsequent stroke (right), for a soil with $\rho_0 = 4000$ Ωm.

In all curves is demonstrated that the increase of the electrode's length results in the decrease of the impulse impedance, up until a length from which this parameter becomes approximately constant. This length corresponds to the effective length. In the plots is also represented the behavior of the low-frequency resistance, that continues to decrease even after reaching the effective length.

It is noticeable that the difference between the values obtained, when considering the frequency dependent soil models and the model with constant soil parameters, increases with the value of ρ_0, which is in agreement with the fact that high-resistivity soils result in higher reductions of the voltage peaks. This difference is also more evident when considering a subsequent stroke.

4) Impulse Coefficient and Effective Length

By using the values of Figs. 13-15, is possible to obtain the curves of the impulse coefficient, which are presented in Figs. 16-18, for the three types of soil and for first and subsequent strokes.

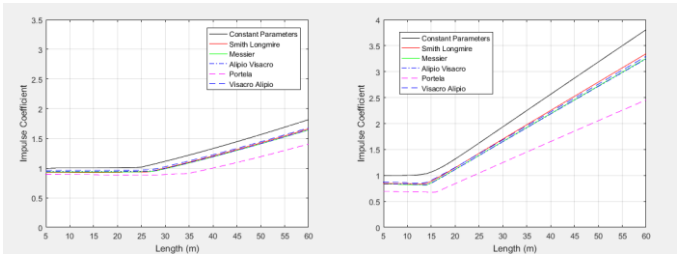

Fig. 16 – Variation of the impulse coefficient with the length of the electrode described in Table 7, subjected to a first stroke (left) and subsequent stroke (right), for a soil with $\rho_0 = 300$ Ωm.

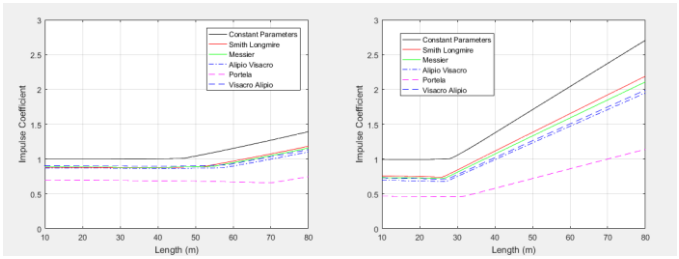

Fig. 17 – Variation of the impulse coefficient with the length of the electrode described in Table 7, subjected to a first stroke (left) and subsequent stroke (right), for a soil with $\rho_0 = 1000$ Ωm.

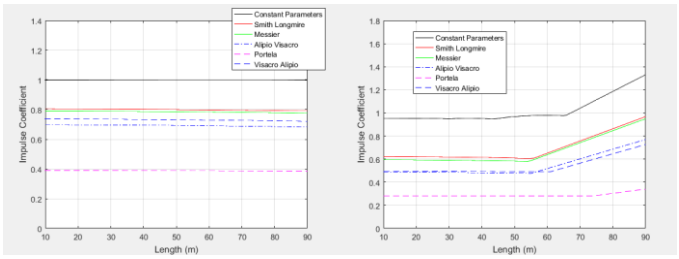

Fig. 18 – Variation of the impulse coefficient with the length of the electrode described in Table 7, subjected to a first stroke (left) and subsequent stroke (right), for a soil with $\rho_0 = 4000$ Ωm.

The results obtained for the impulse coefficient are in accordance with the ones obtained for the impulse impedance, since values smaller than unity are found when considering the frequency dependence, being these values even smaller for high-resistivity soils and for subsequent strokes. Furthermore, after reaching the effective length, the values of the impulse impedance start to increase, since, even though the impulse impedance remains constant, the low-frequency resistance continues to decrease.

As for the effective length, it increases with the value of ρ_0, seeing that the increase of soil resistivity is associated with lower losses along the electrode. Moreover, when comparing the two types of lightning currents, lower effective lengths are found for subsequent strokes, result of the higher losses caused by the higher frequencies. Finally, by comparing the frequency dependent results with the frequency independent model, it

becomes clear that, while the effective length doesn't suffer significant changes for a subsequent stroke, in first strokes, the frequency dependence increases the effective length. This increase is related to the lower attenuations along the electrode, caused by the high values of soil permittivity verified for the range of frequencies that characterize the first strokes, when compared to the ones usually assumed for a frequency independent model.

- *Additional Notes*

Even though the results for the vertical electrode weren´t presented in this paper, its parameters were simulated by the author, being the results in accordance with the ones obtained for the horizontal electrode, with the only difference being the lower values of harmonic impedance verified for the vertical electrode, which causes the GPR, impulse impedance, impulse coefficient and effective lengths to be lower.

Also, all the above results were validated by comparing the simulated plots with the curves presented in [14], where a good agreement was found, being the small differences caused by the different approaches chosen to represent the electrodes, since this work used the transmission-line approach and in [14] is used the hybrid approach (HEM). These results are very important since they show that, by using a simple method, like the transmission-line approach, it is possible to obtain results almost identical to the ones obtained by more complex and rigorous methods, like the hybrid approach, while at the same time requiring less computer power.

Finally, the results also show a good agreement between the response parameters when considering different soil models, except for the Portela model, which used a different set of data than the other models. Even so, the differences between the soil models become more pronounced for high-resistivity soils.

VI. Conclusions

This work presented the most important aspects in the study of the grounding electrode response to lightning currents, having analyzed the impact of the frequency dependence of the soil parameters on this response.

Firstly, from the analysis of the existing soil models, it was possible to verify that all models predict a similar behavior for the soil parameters, being that the rise of frequency causes the reduction of both the values of resistivity and permittivity. It was also possible to observe larger differences, between the soil models, for higher frequencies and values of low-frequency resistivities. After addressing the causality of the models, it was shown that the ones that satisfy the causality tests are: Smith-Longmire, Messier, Portela and Alipio-Visacro. In addition to these models, it was also considered the Visacro-Alipio model, since it is a very common one.

Having chosen the transmission-line approach to represent the electrode and presented the equations that characterize the lightning currents, the equations of the response parameters were obtained. By simulating these parameters in MATLAB, for the values of lightning currents measured at Morro do Cachimbo, is was possible to see that, for a horizontal electrode, the dependency with the frequency results in the reduction of the amplitude of the harmonic grounding impedance and in the intensification of the capacitive effect, when compared to the frequency independent model, being these effects more noticeable for high-resistivity soils.

Furthermore, it was shown that the GPR also suffered a reduction when considering the frequency dependency, being this reduction higher for high-resistivity soils and for subsequent strokes.

As for the variation of the impulse impedance and the impulse coefficient with the electrode's length, it was demonstrated that their values suffer a significant reduction when compared to the frequency independent model, with this reduction being more noticeable for high-resistivity soils and for subsequent strokes. Moreover, it is easy to verify that, for first strokes, the effective length increases when considering the frequency dependence, while for the subsequent strokes the effective length doesn't suffer significant changes.

From all this analysis it can be concluded that, having into consideration the frequency dependence of the soil parameters is essential to correctly represent the behavior of grounding electrodes subjected to lightning currents, since it's parameters are greatly affected by it, even more so when considering high-resistivity soils.

In a way of making this study a more complete and rigorous one, future research must be done so that nonlinear phenomena, such as soil ionization, could be included in the simulations. Also, these studies should also consider stratified soil and be performed for more complex grounding systems, and not only for vertical and horizontal electrodes.

References

[1] J. H. Scott, R. D. Carroll, and D. R. Cunningham, "Dielectric constant and electrical conductivity of moist rock from laboratory measurements," Sensor and Simulation Note 116, Kirtland AFB, NM, Aug. 1964.

[2] J. H. Scott. (1966, May). "Electrical and magnetic properties of rock and soil," Theoretical Notes, Note 18, U.S. Geological Survey [Online]. Available: https://www.ece.unm.edu/summa/notes/Theoretical.html

[3] C. L. Longmire and H. J. Longley. (1973). "Time domain treatment of media with frequency dependent parameters," Theoretical Notes 113, Defense Nuclear Agency, Santa Barbara, CA, USA [Online]. Available: https://www.ece.unm.edu/summa/notes/Theoretical.html

[4] K. S. Smith and C. L. Longmire, "A universal impedance for soils," Defense Nuclear Agency,Alexandria,VA, USA, Topical Report for Period Jul. 1 1975–Sep. 30 1975, 1975.

[5] M. A. Messier, "The propagation of an electromagnetic impulse through soil: Influence of frequency dependent parameters," Mission Res. Corp., Santa Barbara, CA, USA, Tech. Rep. MRC-N-415, 1980.

[6] M. Messier, "Another soil conductivity model," internal rep., JAYCOR, Santa Barbara, CA, 1985.

[7] F. S. Visacro and C. M. Portela, "Soil permittivity and conductivity behavior on frequency range of transient phenomena in electric power systems," presented at the Symp. High Voltage Eng., Braunschweig, Germany, 1987.

[8] C. M. Portela, "Measurement and modeling of soil electromagnetic behavior," in *Proc. IEEE Int. Symp. Electromagn. Compat.*, 1999, vol. 2, pp. 1004–1009.

[9] C. M. Portela and M. C. Tavares, "Modeling, simulation and optimization of transmission lines. Applicability and limitations of some used procedures." IEEE T&D Latin America 2002, Brazil, 38p, 2002.

[10] S. Visacro and R. Alipio, "Frequency dependence of soil parameters: Experimental results, predicting formula and influence on the lightning response of grounding electrodes," in *IEEE Trans. Power Del.*, vol. 27, no. 2, pp. 927–935, Apr. 2012.

[11] R. Alipio and S. Visacro, "Modeling the Frequency Dependence of Electrical Parameters of Soil," in *IEEE Transactions on Electromagnectic Compatibility*, vol. 56, no. 5, pp. 1163–1171, May 2014.

[12] R. Alipio and S. Visacro, "A new model for the frequency dependence of soil parameters," in the 2014 International Conference on Lightning Protection (ICLP), pp. 1432-1436, Dec. 2014.

[13] D. Cavka, N. Mora and F. Rachidi, "A Comparison of Frequency-Dependent Soil Models: Application to the Analysis of Grounding Systems," *IEEE Transactions on Electromagnectic Compatibility*, vol. 56, no. 1, pp. 177-187, Feb. 2014.

[14] R. Alipio and S. Visacro, "Frequency Dependence of Soil Parameters: Effect on the Lightning Response of Grounding Electrodes," *IEEE Transactions on Electromagnectic Compatibility*, vol. 55, no. 1, pp. 132-139, Feb. 2013.

[15] L. V. Bewley, "Theory and tests of the counterpoise," Elec. Engr., vol. 53, pp. 1163-1172, Aug. 1934.

[16] L. V. Bewley, "The counterpoise," G. E. Rev., vol. 37, pp. 73-81, 1934.

[17] P. L. Bellaschi, "Impulse and 60-cycle characteristics of driven grounds - III effect of lead in grounding installation," *AIEE Transactions*, vol. 62, pp. 334-345, 1943.

[18] E. D. Sunde, "Earth conduction effects in transmission systems", Copyright © 1949 by Bell Telephone Laboratories, Inc.

[19] Y. Liu, "Transient Response of Grounding Systems Caused by Lightning: Modeling and Experiments," Ph.D. dissertation, Faculty of Sci. Technol., Univ. Uppsala, Sweden, 2004.

[20] A. P. Meliopoulos and M. G. Moharam, "Transient analysis of grounding systems," *IEEE Trans. Power Apparatus and Systems*, vol. PAS-102, no.2, pp. 389-399. 1983.

[21] A. D. Papalexopoulos and A. P. Meliopoulos, "Frequency dependent characteristics of grounding systems," IEEE Trans. Power Delivery, vol. 2, pp. 1073-1081, October 1987.

[22] M. Ramamoorty, M. M. Babu Narayanan, S. Parameswaran et al., "Transient performance of grounding grids," *IEEE Trans. Power Delivery*, vol. 4, pp. 2053-2059, October 1989.

[23] A. Geri, "Behaviour of grounding systems excited by high impulse currents: the model and its validation" *IEEE Trans. Power Delivery*, vol. 14, no. 3, pp. 1008-1017, July 1999.

[24] A. F. Otero, J. Cidras and J. L. del Alamo, "Frequency-dependent grounding system calculation by means of a conventional nodal analysis technique," *IEEE Trans. Power Delivery*, vol. 14, no. 3, pp. 873-878, July 1999.

[25] J. Cidras, A. F. Otero and C. Garrido, "Nodal frequency analysis of grounding systems considering the soil ionization effect," *IEEE Trans. Power Delivery*, vol. 15, no. 1, pp. 103-107, January 2000.

[26] L. Grcev, "Modeling of grounding electrodes under lightning currents," *IEEE Trans. Electromagn. Compat.*, vol. 51, no. 3, pp. 559–571, Aug. 2009.

[27] L. Grcev and F. Dawalibi, "An electromagnetic model for transients in grounding system," *IEEE Trans. Power Delivery*, vol. 5, pp. 1773-1781, November 1990.

[28] L. Grcev, "Computation of transient voltages near complex grounding systems caused by lightning currents," Proceeding of IEEE 1992 International Symposium on EMC, 92CH3169-0, pp. 393-399.

[29] L. D. Grcev and F. E. Menter, "Transient electromagnetic fields near large earthing systems," *IEEE Trans. Magnetics*, vol. 32, no. 3, pp. 1525-1528, May 1996.

[30] L. D. Grcev, "Computer analysis of transient voltages in large grounding systems," *IEEE Trans. Power Delivery*, vol. 11, pp. 815-823, April 1996.

[31] B. Nekhoul, C. Cuerin, P. Labie, G. Meunier and R. Feuillet, "A Finite Element Method for calculating the electromagnetic fields generated by substation grounding systems," *IEEE Trans. Magnetics*, vol. 31, no. 3, pp. 2150-2153, May 1995.

[32] B. Nekhoul, P. Labie, F. X. Zgainski and G. Meunier, "Calculating the impedance of a grounding system," *IEEE Trans. Magnetics*, vol. 32, no. 3, pp. 1509-1512, May 1996.

[33] F. Dawalibi, "Electromagnetic fields generated by overhead and buried short conductors, Part I – single conductor," *IEEE Trans. On Power Delivery*, vol. PWRD-1, no. 4, pp. 105-111, 1986.

[34] F. Dawalibi, "Electromagnetic fields generated by overhead and buried short conductors, Part II – ground networks," *IEEE Trans. On Power Delivery*, vol. PWRD-1, no. 4, pp. 112-119, 1986.

[35] R. Andolfato, L. Bernardi and L. Fellin, "Aerial and grounding system analysis by the shifting complex images method," *IEEE Trans. Power Delivery*, vol. 15, pp. 1001-1009, July 2000.

[36] S. Visacro, F.H. Silveira, "Evaluation of current distribution along the lightning discharge channel by a hybrid electromagnetic model", *Journal of Electrostatics*, vol. 60, pp. 111-120, 2004.

[37] S. Visacro and J. A. Soares, "HEM: A model for simulation of lightning related engineering problems," *IEEE Trans. Power Del.*, vol. 20, no. 2, pp. 1206–1208, April 2005.

[38] C. Mazzetti and G. M. Veca, "Impulse behaviour of grounding electrodes," *IEEE Trans. Power Apparatus and Systems*, vol. PAS-102, no. 9, pp. 3148-3156, 1983.

[39] R. Velazquez and D. Mukhedkar, "Analytical modelling of grounding electrodes transient behaviour," *IEEE Trans. Power Apparatus and Systems*, vol. PAS-103, no. 6, pp. 1314-1322, 1984.

[40] M. I. Lorentzou, N. D. Hatziargyriou, B. C. Papadias, "Time Domain Analysis of grounding electrodes impulse response," *IEEE Trans. On Power Delivery*, vol. 18, no. 2, pp. 517-524, April 2003.

[41] F. Menter and L. Grcev, "EMTP-Based Model for Grounding System Analysis," *IEEE Trans. On Power Delivery*, vol. 9, pp. 1838-1847, October 1994.

[42] H. B. Dwight, "Calculation of Resistances to Ground," *AIEE Transactions*, pp.1319-1328, December 1936.

[43] S. S. Devgan and E. R. Whitehead, "Analytical models for distributed grounding systems," *IEEE Trans. Power App. Syst.*, vol. PAS-92, no. 5, pp. 1763–1770, October 1973.

[44] R. Alipio, R. M. Costa, R. N. Dias, A. De Conti, and S. Visacro, "Grounding Modeling Using Transmission Line Theory: Extension to Arrangements Composed of Multiple Electrodes," *2016 33rd Int. Conf. Light. Prot.*, pp. 1–5, Sep. 2016.

[45] A. Kuhar, L. Grcev and B. Markovski, "Improved TL Inductivity Formula for Analysis of Grounding Conductors," IEEE EUROCON 2017 – 17th International Conference on Smart Technologies, pp. 908-913.

[46] CIGRÉ WG 33-01, "Guide to Procedures for Estimating the Lightning Performance of Transmission Lines", *CIGRÉ. Technical Brochure*, no. 63, October 1991.

[47] R. B. Anderson and A. J. Eriksson, "Lightning parameters for engineering application," *Electra*, vol. 69, pp. 65-102, 1980.

[48] K. Berger, R.B. Anderson and H. Kroninger, "Parameters of lightning flashes," *Electra*, no. 41, pp. 23-27, July 1975.

[49] S. Visacro, A. Soares Jr, M. A. O. Schroeder, L. C. L. Cherchiglia and V. J. Souza, "Statistical analysis of lightning current parameters: measurements at Morro do Cachimbo Station," *J. Geophys. Res.*, vol. 109, D01105, 2004.

[50] F. Heidler, "Analytische blitzstromfunktion zur LEMP-berechnung," *in Proc. 18th Int. Conf. Lightn. Protec.*, Munich, Germany, pp. 63-66, September 1985.

[51] A. De Conti, S. Visacro, "Analytical representation of single- and double-peaked lightning current waveforms", *IEEE Trans. Electromagn. Compat.*, vol. 49, no. 2, pp. 448-451, May 2007.

[52] A. J. Oliveira, M. A. O. Schroeder, R. A. R. Moura, M. T. C. de Barros, A. C. S. Lima, "Adjustment of current waveform parameters for first lightning strokes: Representation by Heidler functions," *Int. Symp. on Lightn. Protec. (XIV SIPDA)*, Natal, Brazil, October 2017.